



Single-Impact Nonlinear Resonant Acoustic Spectroscopy for Monitoring the Progressive Alkali–Silica Reaction in Concrete

Jiang Jin¹ · Weilun Xi¹ · Jacques Riviere² · Parisa Shokouhi³

Received: 1 February 2019 / Accepted: 24 July 2019 / Published online: 8 August 2019
© Springer Science+Business Media, LLC, part of Springer Nature 2019

Abstract

Alkali–silica reaction (ASR) is a ubiquitous cause of concrete degradation. The reaction produces an expandable gel that may cause internal over-stressing and cracking. This paper demonstrates the utility of single-impact nonlinear resonant acoustic spectroscopy (SINRAS) for monitoring the progress of ASR over the course of a standard ASR-susceptibility test. In SINRAS, the transient softening and subsequent recovery of resonance frequency due to one strong impact are analyzed. The performance of SINRAS in monitoring ASR is compared to that of multi-impact nonlinear resonant acoustic spectroscopy (MINRAS), where the gradual resonance frequency shifts caused by impacts of increasing intensity is measured. The changes in standard linear expansion and linear resonance frequency are recorded in parallel. Finally, the sensitivity of measured parameters to sample temperature is investigated. Our findings indicate that SINRAS, while being much simpler and faster to conduct, yields results that strongly correlate to those from MINRAS and even gives an additional parameter describing the rate of recovery. The extracted nonlinearity parameters exhibit good sensitivity and clearly differentiate between concrete with reactive and non-reactive aggregates. Further, this study suggests that the influence of sample temperature on the nonlinearity parameters depends on the level of ASR progression and has to be taken account.

Keywords Concrete · Alkali–silica reaction · Non-destructive evaluation · Nonlinear acoustics · Nonlinear resonant acoustic spectroscopy

1 Introduction and Background

Alkali silica reaction (ASR) is a prevalent cause of concrete deterioration worldwide. ASR is a deleterious reaction

between metastable forms of silica in some aggregates, and alkali and hydroxide ions in concrete pore solution. The reaction produces a gel that expands upon absorption of moisture, causing internal stresses and microcracking. ASR may lead to the premature loss of strength, serviceability [1] and durability [2]. The two most commonly used test methods to determine the potential alkali reactivity of aggregates are: AMBT or the accelerated mortar bar test (ASTM C1260-14 [3]) and CPT or the concrete prism test (ASTM C1293-08b [4]). Both AMBT and CPT subject standardized (mortar or concrete) samples to severe environmental conditions (i.e., elevated temperature, alkali boosting or saturation in an alkaline bath), promoting the acceleration of ASR. Both tests rely on linear expansion strain as a measure of ASR progress. However, it is widely accepted that CPT produces more reliable results than AMBT, presumably due to the larger specimen size and less severe exposure conditions over a longer time period [5]. While laboratory testing to predict ASR reactivity is fairly established, reliable detection and monitoring of ASR progress in the field remain an outstanding challenge.

✉ Parisa Shokouhi
parisa@psu.edu

Jiang Jin
jjj5395@psu.edu

Weilun Xi
wx5029@psu.edu

Jacques Riviere
jvr5626@psu.edu

¹ Department of Civil and Environmental Engineering, The Pennsylvania State University, 231D Sackett Bldg, University Park, PA 16802, USA

² Department of Engineering Science and Mechanics, The Pennsylvania State University, University Park, PA 16802, USA

³ Department of Engineering Science and Mechanics, The Pennsylvania State University, 412 EES Bldg, University Park, PA 16802, USA

An ideal diagnostic test would provide quantitative and reliable estimation of parameters relevant to the development of ASR products and subsequent cracking. From the practical standpoint, a testing technique is desired that is non-destructive, rapid, economical, and transportable to the field. Over the past decade or so, the application of different non-destructive evaluation (NDE) techniques for detecting ASR has been explored: microwave testing [6, 7], electrical resistivity measurements [8] and linear ultrasonic testing [8–17]. The common observation among the above-listed studies is that the sensitivity of the measured parameters is often obscured by the data variability. This study focuses on nonlinear acoustic testing techniques; an emerging class of NDE methods that have shown great potential for detection of incipient damage and microcracking [18–24], including ASR-induced damage in concrete [16, 25–31]. We introduce a simple resonance-based data collection and analysis methodology and demonstrate its effectiveness in monitoring CPT specimens.

Nonlinear acoustic/ultrasonic testing is well suited to evaluate ASR because modification in concrete microstructure is expected to change the second or higher order strain-dependency of the materials elastic properties and thus, to influence the acoustic/ultrasonic wave propagation. Micro-cracks introduce a discontinuity in strain field. Acoustic/ultrasonic perturbation beyond a certain strain threshold ($\sim 10^{-6}$), cause microcracks to close, and also crack faces to clap and/or slide against each other. Therefore, at any instance during the nonlinear acoustic/ultrasonic test, each microcrack may be open, closed, or in transition between the two states. Since the elastic modulus at each strain instant depends on the instantaneous fraction of open versus closed cracks [32], a medium containing microcracks exhibits increased strain-dependency of elastic modulus or nonlinearity. The acoustic/ultrasonic waves propagating in a nonlinear elastic medium will be distorted, resulting in specific nonlinearity signatures such as generation of higher harmonics of the incident wave frequency as well as strain-dependency of wave speed, attenuation and resonance frequency. Each nonlinear acoustic/ultrasonic NDE technique is based on measuring specific nonlinearity parameters that capture one or more of these signatures. Empirical observations attest to the high sensitivity of nonlinearity parameters to the presence of microcracks in a wide spectrum of materials, as summarized in [33]. Even a small population of microcracks can result in manifold rise in nonlinearity [33]. The higher the microcrack density, the larger is the expected increase. However, there seems to be a threshold on the size (i.e., crack aperture) of a “nonlinear crack”, beyond which the cracks do not contribute to nonlinearity [34]. Intuitively speaking, cracks of wider apertures cannot be activated by perturbations caused by nonlinear elastic acoustic/ultrasonic waves.

In this paper, we use impact-based nonlinear resonance acoustic spectroscopy (INRAS). The choice of method is motivated by (1) its similarity to the familiar concrete degradation test prescribed by ASTM C215 [35] and (2) the fact that resonance-based testing provides a global estimate of sample nonlinearity and thus, is ideal for assessing volumetrically damaged materials. This method relies on measuring the strain-dependency of resonance frequencies obtained at different levels of excitation. The resonance frequency of a linear elastic material is strain-invariant. In contrast, materials with mesoscopic nonlinearity [36] exhibit strain-dependent resonance frequencies: at higher amplitudes, the material exhibits transient elastic softening. As a result, resonance frequencies shift downward towards lower frequencies. However, the shift is reversible i.e., if we wait long enough, the disturbed material slowly relaxes and the resonance frequency gradually recovers (slow dynamics) [31]. For a predominantly hysteretic nonlinear elastic material such as mortar or concrete, a linear dependence of the relative resonance frequency shift on the driving strain amplitude ($10^{-6} < \varepsilon < 10^{-5}$) is expected [37]. The coefficient of proportionality is the hysteretic nonlinearity parameter α :

$$\frac{\Delta f}{f_0} = \frac{f - f_0}{f_0} = -\alpha(\varepsilon - \varepsilon_0), \quad (1)$$

where, f_0 is the linear resonance frequency measured at the lowest strain amplitude above the noise threshold ε_0 and f is the resonance frequency at a higher strain amplitude ε . Materials with no or little hysteretic nonlinearity (e.g., aluminum alloys) exhibit very low $\alpha \approx 0$, whereas those with high hysteretic nonlinearity are characterized with large α . The higher the density of microcracks, the higher is the expected nonlinearity and consequently, the larger is the value of α .

In this study, INRAS is employed to monitor the evolution of nonlinearity in concrete prisms over the course of the ASR susceptibility test CPT. INRAS can be performed either with multiple impacts or single impact. The multi-impact NRAS, or MINRAS (also known as NIRAS [26, 30]) involves application of several mechanical impacts of increasing strength, while single-impact NRAS, or SINRAS (also known as NSIRAS [19], INRS [38], and FANSIRAS [39]) only requires one strong impact. Compared to the conventional nonlinear resonant acoustic spectroscopy (conventional NRAS), which typically uses a PZT as the source of excitation, MINRAS offers the advantages of being simple, fast, transportable and economical. However, there are concerns about (1) the effect of potential damage due to multiple hammer strikes and (2) the timing between successive impacts and role of slow dynamics in corrupting the test results. In this paper, we first demonstrate that MINRAS and conventional NRAS can yield very similar

Table 1 Mortar and concrete mixture design

Mixtures	Portland cement (type I) (kg/m ³)	w/c	Water (kg/m ³)	Sand (kg/m ³)	Coarse aggregate (kg/m ³)
Mortar (river)	584.8	0.47	294.4	1315.8	–
Concrete					
Glass	420.0	0.45	193.5	687.5	1032.7
Oley	420.0	0.45	197	742.5	1032.7

results. Next, we compare the results from MINRAS on CPT concrete specimens to those from SINRAS, where the reverberation response to a single albeit sufficiently strong impact (strain $\sim 10^{-5}$) is analyzed. The SINRAS is simpler and faster to conduct and does not evoke the aforementioned concerns associated with MINRAS. Finally, the influence of specimen temperature on the extracted parameters is evaluated. In addition to the nonlinear acoustic parameters, linear expansion strain is measured in parallel to allow comparisons between ASR progress and nonlinear measures.

The rest of the paper is organized as follows. A description of test specimens and methods is given in Sect. 2. In Sect. 3, we first compare conventional NRAS versus MINRAS on a mortar sample, then compare SINRAS and MINRAS in monitoring ASR growth of concrete prisms with aggregates of different reactivity. The results of temperature sensitivity investigation are also presented in Sect. 3. In the end, the paper is concluded by a discussion of the main observations and perceived limitations in Sect. 4 followed by conclusions in Sect. 5.

2 Materials and Methods

This study presents the test results pertaining to one set of standard concrete prisms made with two different aggregates prepared for CPT. Linear expansions of the prisms were measured following the standard procedures. The evolution of linear resonance frequency f_0 and non-classical nonlinearity parameters in each prism was monitored using two different versions of impact-based NRAS: MIRAS and SINRAS. In addition to concrete prisms, a smaller prismatic mortar bar was cast and tested. We have chosen a small mortar sample, because conducting NRAS on a large concrete prism is impractical due to the need for a high-power excitation source. The smaller dimensions of the mortar bar allowed us to directly compare conventional NRAS and MINRAS as will be demonstrated in Sect. 3.1.

2.1 Sample Composition and Preparation

2.1.1 Mortar Bar for Conventional NRAS Versus MINRAS Comparison

A prismatic mortar bar of dimensions $25.4 \times 25.4 \times 286 \text{ mm}^3$ ($1 \times 1 \times 11.25 \text{ in.}^3$) with potentially medium reactivity sand (River) was prepared according to ASTM C1260-14. After being cast and moist cured for 24 h, the sample was immersed in water and placed in an oven at $80 \text{ }^\circ\text{C}$ ($176 \text{ }^\circ\text{F}$) for 24 h. To promote ASR, the mortar bar was later immersed in a 1 N NaOH solution at $80 \text{ }^\circ\text{C}$ ($176 \text{ }^\circ\text{F}$) for 10 days before being taken out for testing. Table 1 provides additional details on the mortar mixture.

2.1.2 Concrete Prisms for MINRAS and SINRAS

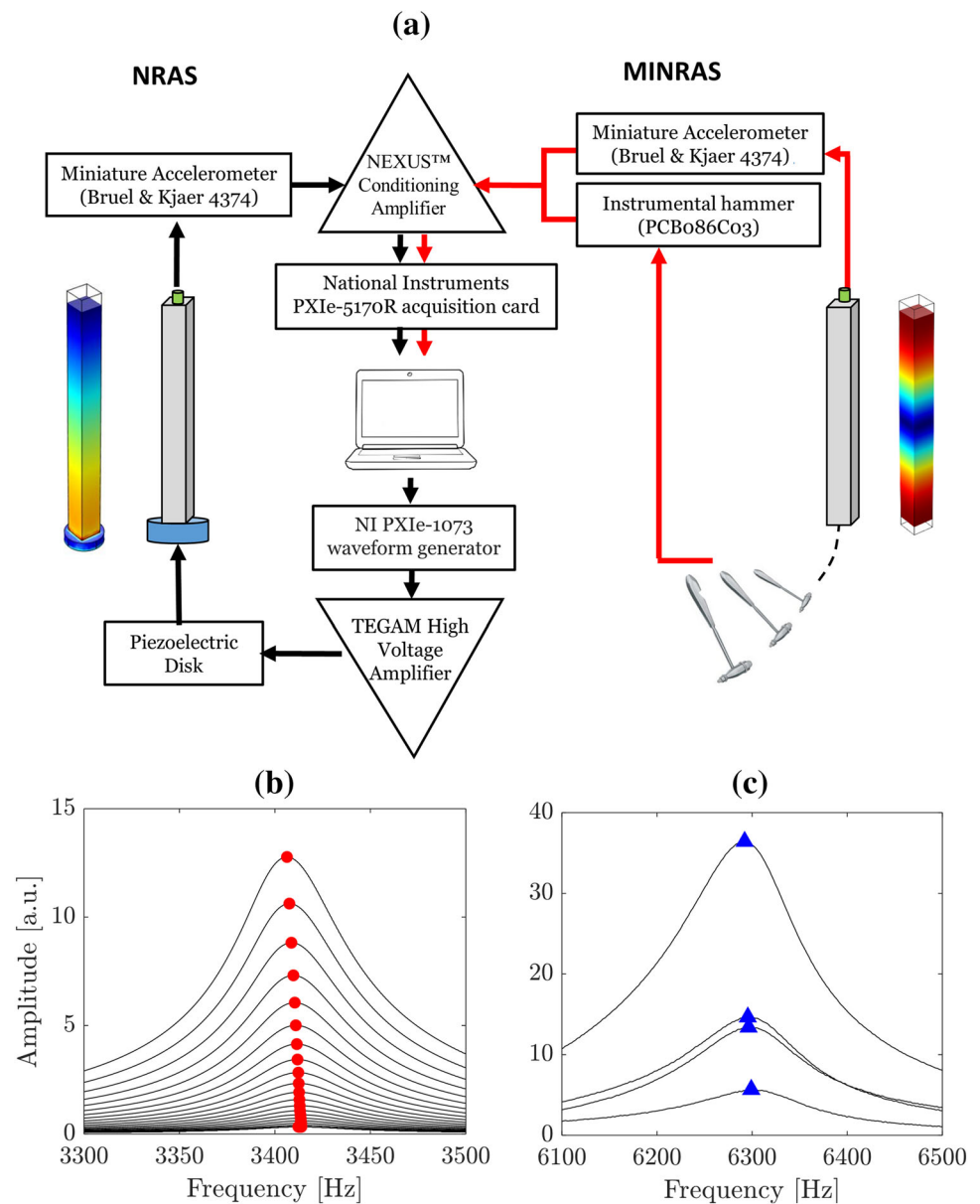
Two concrete mixtures with sand of potentially low (designated as “Oley”) and high (designated as “Glass”) reactivity levels were prepared following the guidelines of ASTM C1293-08b. The low reactivity natural sand is from a source in Oley, PA. Non-reactive crushed stone was used as the coarse aggregate and the alkali content of cement was boosted to 1.25% $\text{Na}_2\text{O}_{\text{eq}}$. The two mixtures were designed to have similar water-to-cement (w/c) ratios. From each mix, four prisms of dimensions $76.2 \times 76.2 \times 286 \text{ mm}^3$ ($3 \times 3 \times 11.25 \text{ in.}^3$) were cast, moist cured for 24 h, and stored over water in sealed containers at $38 \text{ }^\circ\text{C}$ ($100.4 \text{ }^\circ\text{F}$) and 100% relative humidity. Out of a set of four prisms per mixture, three were used for expansion measurements and one for MINRAS and SINRAS.

2.2 Test Methods

2.2.1 Linear Expansion

Linear expansion of concrete prisms was measured with an accuracy of 0.0001 inches (0.00254 mm) following the procedures prescribed by ASTM C1293-08b. The initial comparator readings were taken shortly after demolding. The 36 subsequent measurements were made at intervals of 3 to 14 days. The reported expansions are the averaged readings from three prisms at each age. The measurements were termi-

Fig. 1 a Schematic test setups used for NRAS and MINRAS on a mortar sample shown in left and right panels, respectively; **b** typical NRAS frequency spectra; and **c** typical MINRAS frequency spectra on the mortar sample



nated after 186 days, when the expansions for Oley reached a plateau as will be shown in Sect. 3.2.

2.2.2 Conventional NRAS and MINRAS on Mortar Bar

Conventional NRAS was conducted on a prismatic mortar bar and the results are compared to those from MINRAS. NRAS test setup is similar to that used for linear resonance frequency measurements; however, instead of using a frequency sweep at one very low amplitude ($\varepsilon < 10^{-6}$), the resonance frequencies f at larger excitation amplitudes ε are also measured. A schematic representation of the experimental setup used is shown in Fig. 1a-left panel. A large piezoelectric ceramic (American Piezo Ceramics) with a diameter of 45 mm and thickness of 7 mm was glued (Phenyl salicylate, 99%) to one

end to excite the sample at its first compressional mode and a miniature accelerometer (Bruel & Kjaer 4374) to the other end of the specimen. A heavy piece of steel (weight $> 10 \times$ the weight of the specimen) was epoxy glued to the other side of the piezoelectric ceramic to ensure efficient excitation of the sample. Consequently, it is safe to assume that the sample had fixed-free boundary condition. A series of sinusoidal chirps (with duration of 3 s and linearly swept through 2400–3200 Hz) generated by NI PXIe-1073 arbitrary waveform generator and amplified ($\times 50$) using a TEGAM high-voltage amplifier were used to drive the piezoelectric disk. After completing each sweep and waiting for a sufficient amount of time to allow relaxation, the input voltage was raised to the next prescribed level. At each driving amplitude, the acceleration was amplified [$1 \text{ mV}/(\text{ms}^{-2})$] using a

NEXUS™ conditioning amplifier and recorded by NI PXIe-5170R acquisition card at a sampling frequency of 1 MHz. The data acquisition process was fully automated using LabVIEW running on a laptop. The MINRAS setup for mortar is similar to NRAS, except using an instrumented hammer as the source of perturbation to excite the first compressional mode with a free–free boundary condition (Fig. 1a-right panel). We manually applied 10 hammer impacts, among which only those strikes with incremental strain amplitude are kept to reduce the influence of ‘conditioning’. In other words, those strikes with a strain amplitude smaller than any of the previous strikes are removed. Although NRAS and MINRAS are conducted with different boundary conditions, this comparison is valid for a homogeneous sample.

The outputs of NRAS (Fig. 1b) and MINRAS (Fig. 1c) consist of a series of frequency spectra corresponding to different driving amplitudes. The resonance frequency f in each spectrum is the frequency corresponding to the maximum spectral amplitude. In order to achieve improved frequency resolution, the recorded acceleration histories were zero-padded and the frequency peak in each spectrum was fit by a parabolic function. The maximum strain within the sample at each amplitude was estimated from the measured acceleration [40]. The formulae for estimating strain amplitude from conventional NRAS and MINRAS are shown in Eqs. 2a and 2b, respectively.

$$\varepsilon_{max} = -\ddot{u}_{max}/(8\pi Lf^2) \quad (\text{Fix - Free, NRAS}), \quad (2a)$$

$$\varepsilon_{max} = -\ddot{u}_{max}/(4\pi Lf^2) \quad (\text{Free - Free, MINRAS}), \quad (2b)$$

where L is the sample length. The data analysis involves plotting the relative shift in resonance frequency versus the maximum strain and estimating α (Eq. 1) from linear regression.

2.2.3 MINRAS on Concrete Prisms

Our MINRAS test configuration for concrete prisms is similar to the standard method for determining the dynamic modulus of concrete (ASTM C215 [35]). The concrete prism was supported by soft foam to simulate free–free boundary conditions. An instrumented hammer (PCB 086C03) was used to manually strike the sample at its center in order to excite the first transverse flexural mode of vibration (Fig. 2a-right panel). Either a laser Doppler vibrometer (Polytec OFV-525 sensor head & OFC-5000 controller) or a miniature accelerometer (Bruel & Kjaer 4374) was used to record the vibrational response at one end of the sample. The recorded signal was amplified and digitized at a sampling frequency of 1 MHz.

MINRAS requires multiple strikes of varying intensity that range from very gentle ($\varepsilon < 10^{-6}$) to relatively strong ($10^{-6} < \varepsilon < 10^{-5}$). The wait time between consecutive strikes should be long enough to minimize the effects of conditioning on the test results [41]. For each set of MINRAS, we manually applied 30 hammer impacts, out of which only those with monotonically increasing amplitudes are included in the subsequent analyses to reduce the influence of ‘conditioning’. The very gentle first impact gives the reference linear resonance frequency f_0 . The subsequent resonance frequencies become smaller with the increasing strain amplitude. Typical MINRAS amplitude spectra corresponding to multiple impacts are shown in Fig. 2d. The maximum strain can be estimated from the measured acceleration using the following relationship [23]:

$$\varepsilon_{max} = \frac{0.219\pi(3.0112)^2 D}{8f^2\sqrt{12}L^2} \ddot{u}_{max}, \quad (3)$$

where D is the sample width. The nonlinear parameter from MINRAS α_{MINRAS} is estimated from Eq. 1.

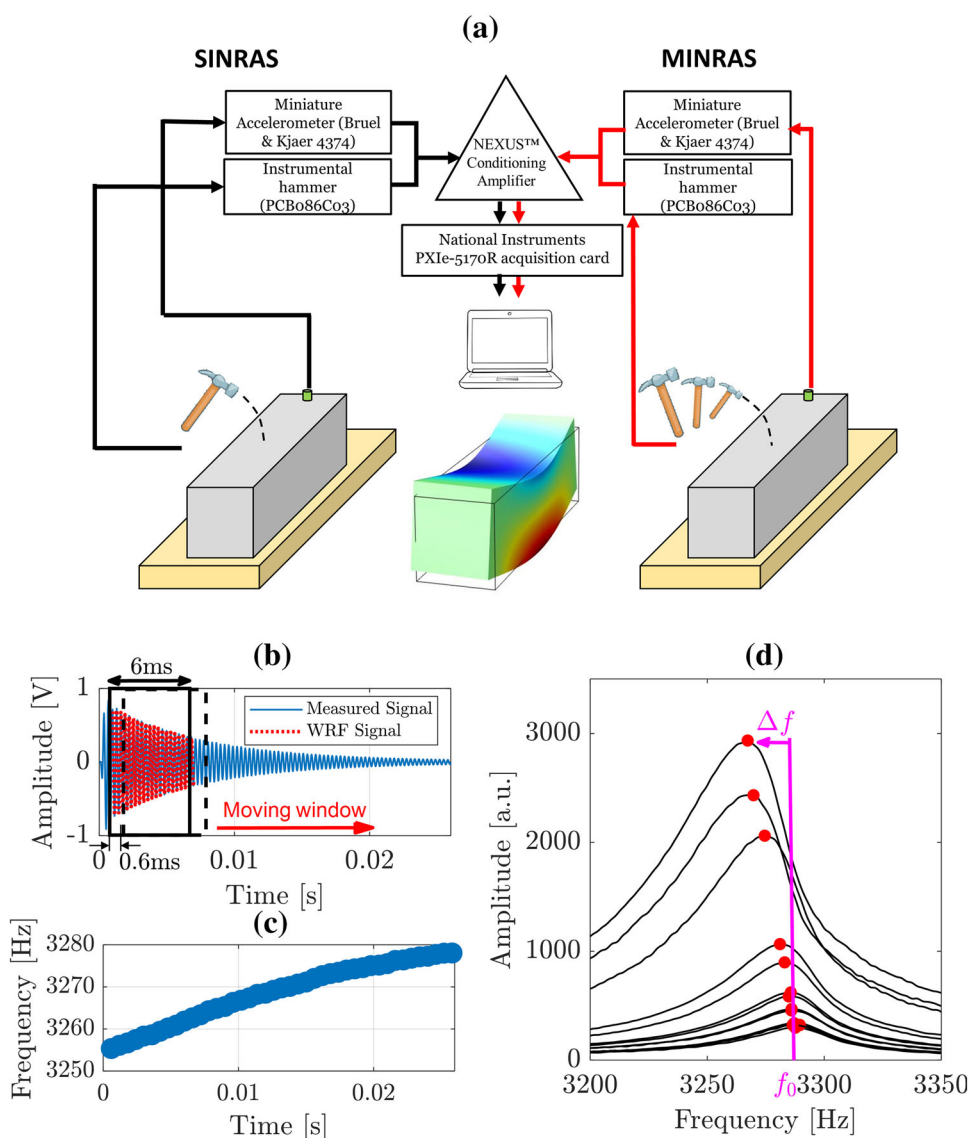
2.2.4 SINRAS on Concrete Prisms

The test setup for SINRAS is similar to that of the previously described MINRAS except that the test protocol requires only one albeit sufficiently strong ($\varepsilon > \sim 5 \times 10^{-6}$) impact (Fig. 2a-left panel). The impact results in an instantaneous, but transient drop in the resonance frequency of the sample. As the sample rings down (Fig. 2b), the resonance frequency slowly recovers (Fig. 2c). Nonlinearity of the sample is estimated from the initial drop and the recovery rate of the resonance frequency.

Data analysis for SINRAS is very different from that for MINRAS; it includes determining the changing frequency content of the response. We used windowed reverberation fitting (WRF) [23] to analyze the ring down; similar results are expected using Short Time Fourier transform [19] or Hilbert Huang Transform [18]. WRF uses a sliding window to capture the changing frequency content in the amplitude-decaying time signal. As shown in Fig. 2b, the window size was selected to be 6 ms with a step size of 0.6 ms corresponding to a 90% overlap between adjacent windows. Given the average resonance frequency of around 3000 Hz, each window contained about 18 full reverberation cycles. The decaying signal in each window was described by an exponentially decaying sinusoidal. Assuming constant frequency and damping within each window, the signal contained in the k^{th} window was modeled as follows:

$$x_k(t) = A_k e^{-\theta_k t} \sin(2\pi f_k t + \varphi_k) \quad k = 1, 2, \dots, n, \quad (4)$$

Fig. 2 **a** Schematic test setups used for SINRAS and MINRAS on concrete prisms shown in left and right panels, respectively; **b** typical ring-down signal and Windowed Reverberation Fitting (WRF) in one specific window; **c** the resulting estimated temporal variation of resonance frequency; and **d** typical MINRAS frequency spectra on concrete prisms



where $A_k, \theta_k, f_k, \varphi_k$ are the maximum amplitude, ‘instantaneous’ damping, resonance frequency, and phase shift of the signal within the k th window, respectively. The amplitude A_k is later used to estimate the decaying strain ε_k over the duration of the signal using Eq. 3. Figure 2c shows an exemplary evolution of resonance frequency with time for Oley after 98 days of exposure. The material shows an immediate softening just after the hammer strike. This softening is however, only transient; once the impact-induced perturbation is over, the dynamic elastic modulus recovers slowly towards the unperturbed modulus due to conditioning and slow dynamics, which is a signature of materials with hysteretic nonlinearity [37].

In addition to the transient softening, we also study the recovery of the resonance frequency after perturbation. The soft ratchet model proposed by Vakhnenko [42] and experimental work on a variety of materials [43] suggests a time

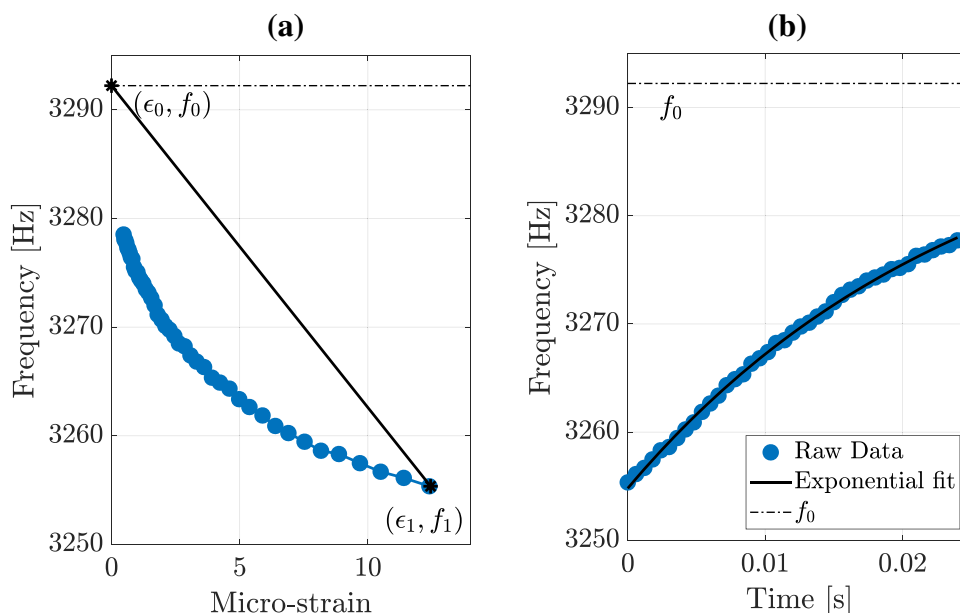
logarithmic recovery of elastic modulus equivalent to a continuous distribution of exponential recoveries. However, our measurements in this study (see Fig. 3b) and a previous study on concrete undergoing freeze–thaw damage lend themselves to a better fit with a single exponential function [18]:

$$\frac{f - f_0}{f_0} = Ae^{-\nu t}, \tag{5}$$

where f_0 is the reference linear resonance frequency, parameter ν describes the recovery rate. In other words, a single exponential function dominates the recovery spectrum. Following Eq. 5, the instantaneous resonance frequency can be written as a function of time as follows:

$$f = Af_0e^{-\nu t} + f_0 \tag{6}$$

Fig. 3 **a** Calculation of nonlinear parameter α_{SINRAS} from SINRAS response: ϵ_1 and f_1 are the strain and resonance frequency within the first window, while f_0 is the resonance frequency at $\epsilon_0 = 0$ obtained from curve fitting; **b** temporal resonance frequency superimposed by the soft ratchet exponential fit. The data corresponds to Oley after 98 days of exposure



The parameters $A, f_0,$ and ν are identified with curve fitting using trust-region-reflective least squares algorithm. The nonlinearity parameter from SINRAS α_{SINRAS} is defined as follows:

$$\alpha_{SINRAS} = -\frac{(f_1 - f_0)/f_0}{\epsilon_1 - \epsilon_0} \tag{7}$$

where f_1 is the resonance frequency during the first window (with maximum strain ϵ_1), and f_0 is the resonance frequency at $\epsilon_0 = 0$ that obtained from curve fitting, Fig. 3a shows an example of calculating α_{SINRAS} .

3 Results

3.1 Comparison Between Conventional NRAS and MINRAS for a Mortar Bar

As the first step, to demonstrate the agreement between conventional NRAS and MINRAS, one mortar bar was tested using both methods. A comparison of the test results is shown in Fig. 4. First, we observe an overall linear relation between strain and the relative frequency shift, as predicted by the nonlinear hysteretic model (Eq. 1). Second, we find that the two tests yield very similar outcomes: the measured α from NRAS is approximately 333 compared to 314 from MINRAS. Note that the different boundary conditions, *fixed-free* boundary conditions for NRAS versus *free-free* for MINRAS, account for the doubling of the resonance frequencies in MINRAS spectra.

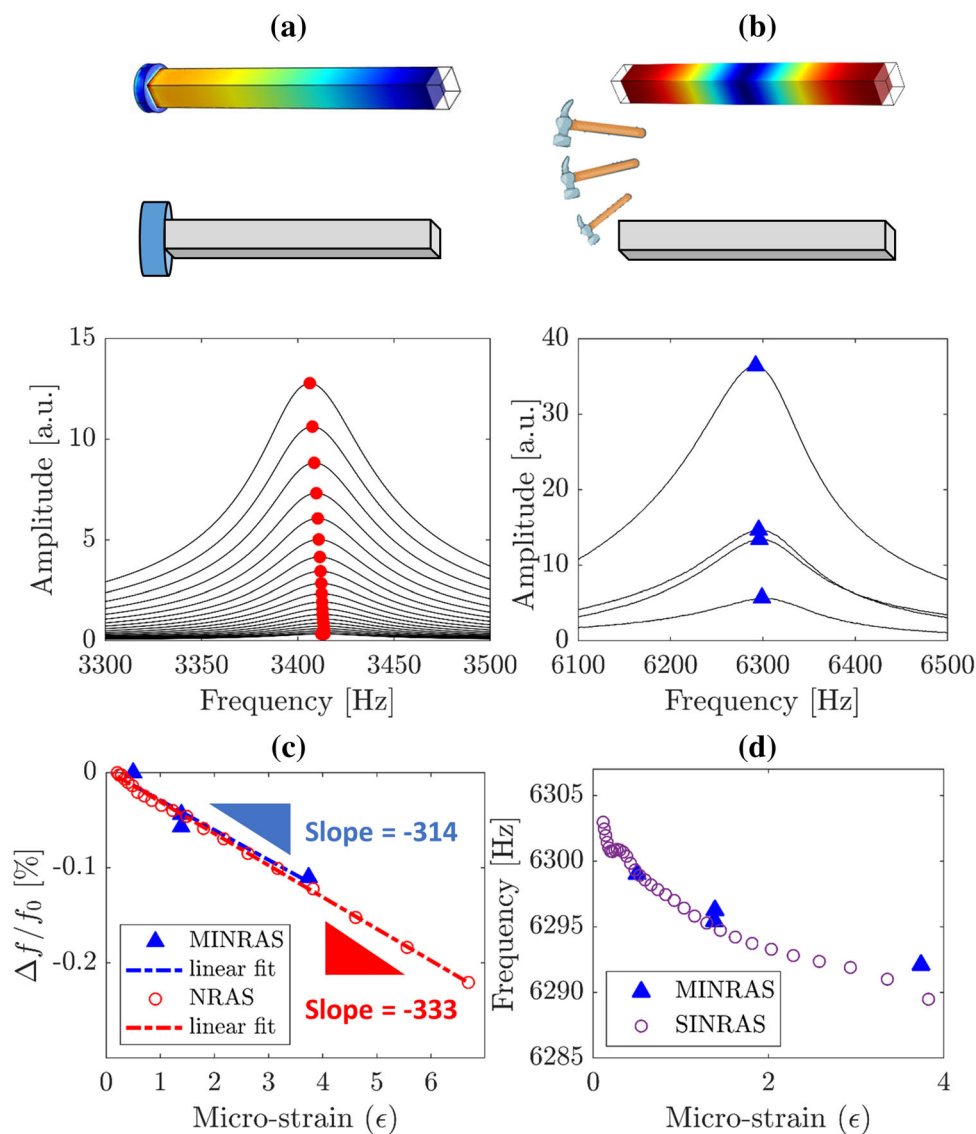
3.2 Linear Expansion

Expansion measurement results for concrete prisms containing Oley and Glass sands are compared in Fig. 5. As expected, prisms made with Glass sand expanded much faster and significantly more than those with Oley sand. The expansion values for Oley and Glass samples after 186 days were 0.036% and 1.366%, respectively. The expansion of Glass sample surpassed the threshold value for deleterious expansion (0.04%, 1 year after casting) after only 15 days. Therefore, glass sand is classified as very highly reactive. The expansion of Oley sample approached but did not exceed the deleterious threshold over the 186 days. Longer term measurements up to 1 year is needed to determine whether this aggregate can be classified as non-reactive [44].

3.3 MINRAS on Concrete Prisms

MINRAS was conducted on the two concrete prisms with Oley and Glass sands. The testing was carried out every 3–14 days during the course of CPT: Oley samples were tested for 172 days, while measurements on Glass samples were terminated after only 30 days due to excessive damage. To investigate the influence of temperature, MINRAS and SINRAS on the concrete prisms was done at two temperatures: 38 °C (‘hot’) and 23 °C (‘cold’). The first set of measurements (hot) were taken within 30 min and the second set (cold), about 24 h after removing the specimens from the oven. Except when taken out for testing, the specimens remained over water in sealed containers. As such, no significant change in relative humidity is anticipated. The reported values here correspond to the measurements taken at 23 °C (i.e., cold), the same temperature at which the linear expansion

Fig. 4 Frequency spectra for a mortar bar obtained from: **a** conventional NRAS and **b** MINRAS. The corresponding relative resonance frequency shift versus strain curves are compared in **(c)** for NRAS versus MINRAS, and **d** MINRAS versus SINRAS corresponding to the largest impact



sion (Sect. 3.2) was measured. The influence of temperature on the measured parameters is discussed in Sect. 3.6.

3.3.1 The Evolution of Nonlinear Parameter α_{MINRAS}

The evolution of α_{MINRAS} for the two prisms is compared in Fig. 6. The first observation is that α_{MINRAS} for the prism with Glass sand grows at a much faster rate, compared to the sample with Oley sand. This is consistent with the expansion results shown in Fig. 5 that indicate a much higher reactivity for Glass sand. The nonlinearity of Glass prism increases by 772% after only 30 days of exposure, orders of magnitude more than the increase in α_{MINRAS} for the sample with Oley sand. The evolution of α_{MINRAS} for the concrete prism with Oley sand follows a distinct trend: the initial slight decrease in α_{MINRAS} (Phase I: days 0 to 19) is followed by a sharp increase until about Day 60 (Phase II), after which α_{MINRAS}

fluctuates for about 50 days until about Day 110 (Phase III) and finally, slowly decreases (Phase IV).

The temporal evolution of nonlinearity parameter for Oley sample (Fig. 6) is consistent with the previously reported MINRAS results on mortar and concrete [26, 30, 45, 46]. We argue that hydration products reducing the microscopic porosity at an early age could be the reason why we observe an initial slight decrease in α_{MINRAS} . At a later age, the likely accumulation of microcracks results in the observed increase in nonlinearity. After reaching a maximum value, the nonlinearity of the Oley sample fluctuates and eventually decreases. This change of trend occurs around the time when linear expansion approaches a plateau. The underlying mechanisms of the observed late-age drop in nonlinearity are not well understood. Chen et al. [30] attributed this behavior to the formation of crystalline products within the ASR gel due to interactions with calcium ions or carbonation, resulting in an

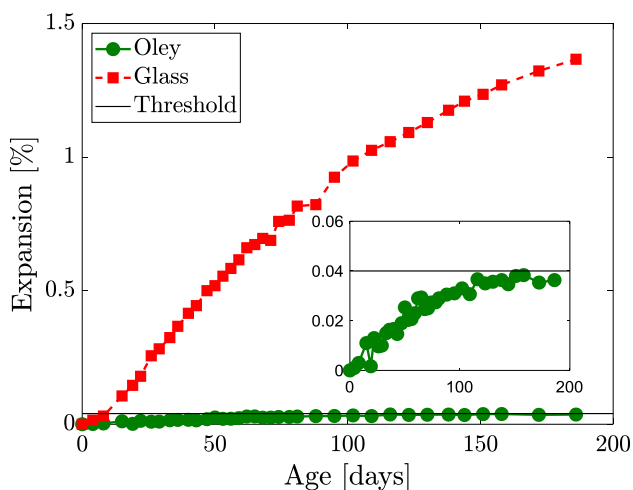


Fig. 5 Expansion results for concrete prisms containing Oley or Glass sand. The black horizontal line marks the corresponding reactivity thresholds prescribed by ASTM C1293-08b (0.04%)

overall stiffening. The relatively harsh storage environment (38 °C, 100% RH) prescribed by ASTM C1293 may also play a role: the high humidity and availability of water, condenses moisture on the surface of the concrete prisms, drawing the OH⁻ and alkali ions out of concrete pore solution, thus slowing down ASR manifested by the plateauing of expansion [47]. Finally, it has been argued that the continued formation and expansion of ASR gel can lead to filling of the existing micro-cracks with reaction product and widening them beyond a critical size, resulting in a decrease of nonlinearity [30]. This latter argument is however, an unlikely scenario here considering that linear expansion does not increase but

remains almost constant over the period of time when the nonlinearity decreases.

3.3.2 The Evolution of Linear Resonance Frequency f_0

The measurement of f_0 is an integral part of MINRAS as f_0 corresponds to the resonance frequency at the smallest amplitude impact. As shown in Fig. 7, f_0 evolves differently for the two concrete prisms during the course of CPT. The linear resonance frequency f_0 for the Glass sample starts to decrease sharply after a few days of exposure and shows about 18% loss after only 30 days. In contrast, f_0 for the prism with Oley sand evolves differently over the four phases previously identified for the progress of the nonlinear parameter; it increases sharply in Phase I, slightly decreases in Phase II, reaches a plateau in Phase III and finally, slightly increases in Phase IV as depicted in Fig. 7.

The sharp monotonic decrease of f_0 for Glass sample is similar to the trend observed for highly reactive samples by Rivard and Saint-Pierre [8]. It suggests substantial formation of ASR gel and subsequent cracking within the sample. The more compliant ASR products within the otherwise stiff surrounding concrete result in a reduced effective elastic modulus and consequently, lower resonance frequency f_0 . Similar to the evolution of α_{MINRAS} , the f_0 for prisms with Oley sands show a four-phase behavior. The initial sharp increase of f_0 in Phase I is most likely caused by the early age densification of microstructure due to cement hydration. The following subtle decrease in Phase II is presumably because of the competing influence of ASR products. Around the time when the expansion of Oley sample reaches a plateau, the

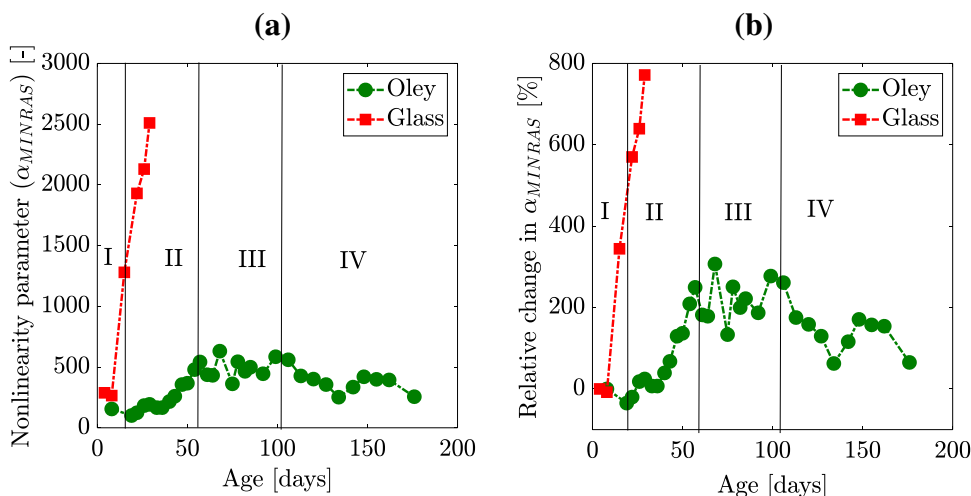
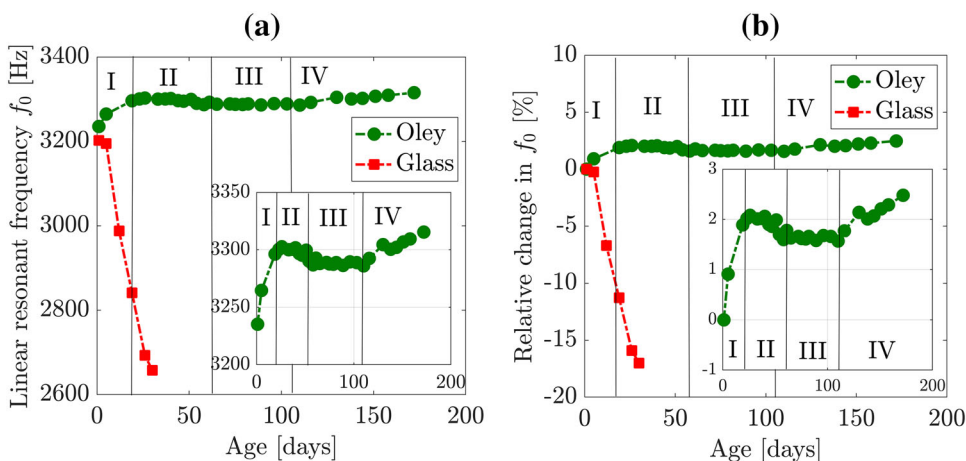


Fig. 6 The evolution of hysteretic nonlinearity parameter from MINRAS α_{MINRAS} for two concrete prisms made with Oley and Glass sands presented in terms of: **a** absolute values; and **b** percentage change. Note the manifold increase in α_{MINRAS} for the Glass sample over the first

few days of exposure. The vertical lines mark four different phases of evolution for the Oley sample, where the nonlinearity slightly decreases (Phase I), increases (Phase II), fluctuates (Phase III) and shows a decaying trend (Phase IV)

Fig. 7 The evolution of linear resonant frequency with exposure time (age) for concrete prisms presented in the form of **a** absolute values; and **b** percentage change. The vertical lines mark the four different phases identified in the evolution trend of f_0 for Glass and Oley samples



mechanisms that increase the elastic modulus prevail, resulting in slight but monotonically increasing f_0 . The observed evolutions of f_0 for Glass and Oley samples suggest that this parameter may not be sensitive enough to micro-damage development unless the damage density exceeds a certain threshold.

3.4 SINRAS Versus MINRAS

A comparison between MINRAS and SINRAS measurements is given in Fig. 8. The SINRAS results correspond to three selected impacts of ‘High’, ‘Medium’, and ‘Low’ strengths chosen among the impact strikes for the MINRAS test. First, we observe that the resonance frequencies corresponding to the largest strain in a SINRAS do not match the resonance frequency for the same hammer strike in MINRAS. This offset is a result of applying FFT to the entire reverberation signal when analyzing MINRAS data. FFT provides the averaged frequency content at each strain amplitude and therefore, systematically overestimates the resonance frequencies at higher strains leading to a systematic underestimation of α_{MINRAS} . One way to correct this offset is to apply FFT to a short-windowed portion of the signal (0.6 ms long) that captures only the beginning of the reverberation. A comparison between the results of the standard FFT analysis of MINRAS data and the suggested corrective approach is included in Fig. 8. For the data presented in this figure, the corrected and uncorrected α_{MINRAS} values are 745 and 584, respectively.

A second observation in Fig. 8 is that the SINRAS recoveries (circular markers) are not linear and fall under the corrected multi-impact curve (triangular markers). In fact, the combination of corrected MINRAS and SINRAS results resembles a hysteretic constitutive relationship: the resonance frequency-strain plot of multi-impact testing corresponds to the loading phase, while single-impact recoveries represent the unloading phase. The hysteretic behavior

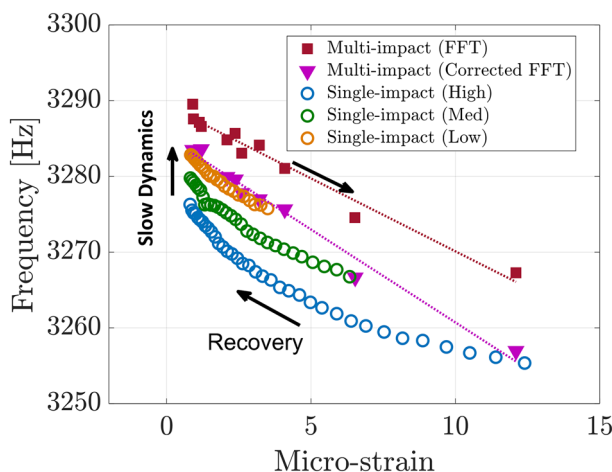
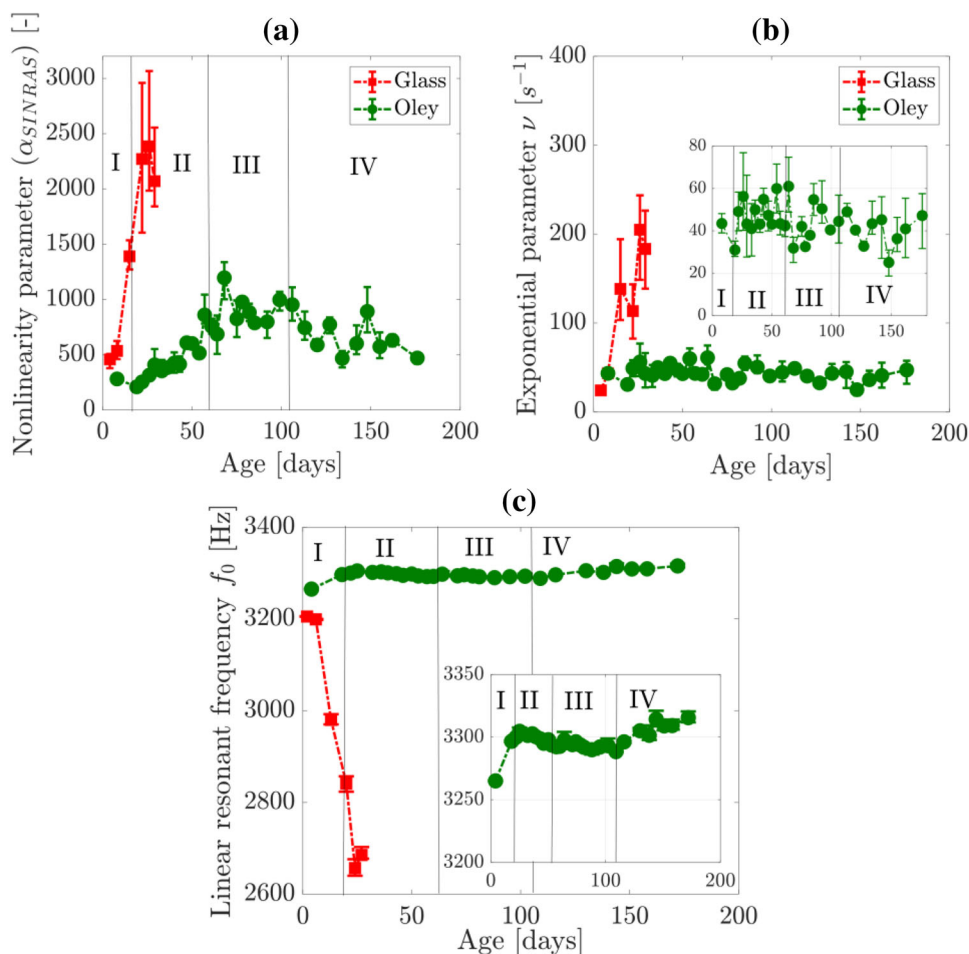


Fig. 8 Comparisons between MINRAS (square markers), corrected MINRAS (triangular markers), and SINRAS (circular markers) for three different impacts of high (high), medium (med) and low (low) strength. The exemplary data presented in this figure pertains to Oley specimen after 98 days of ASR exposure. Note the closed loops formed by the corrected MINRAS data (when FFT is performed on a small window corresponding to large strain at the beginning of the ring-down) and SINRAS data. The hysteretic behavior is similar to what would be observed with a quasi-static mechanical test, where MINRAS (SINRAS respectively) data corresponds to the loading (unloading) phase

observed in Fig. 8 paradoxically implies that the nonlinear hysteretic model (Eq. 1) is not strictly valid, since a linear relation is expected between frequency and strain. This discrepancy arises from slow dynamic (time-dependent) effects that are not accounted for by this model [48]. In addition, the resonance frequency tends not to drop as fast as the decaying of strain amplitude during the beginning of the ring-down, because the vibration is still conditioning the sample. While during the later part of the ring-down, the amplitude of the vibration is much smaller, therefore the influence of conditioning is much less, and the rate of frequency recovery catches up with the rate of strain decaying.

Fig. 9 **a** The evolution of hysteretic nonlinearity parameter from SINRAS α_{SINRAS} for two concrete prisms made with Oley and Glass sands; **b** The comparison between the evolution of the recovery rate ν for samples Oley and Glass. **c** The evolution of linear resonant frequency f_0 extracted from SINRAS. The vertical lines mark the four different phases



Finally, we observe in Fig. 8 that for the largest impacts, the frequency at the end of the ring-down is still lower than the one measured at low strain amplitude for MINRAS data (f_0). This is again due to slow dynamics effects: the sample is not fully recovered when the ring-down ends and it may take minutes/hours to reach full recovery. The evolution of α_{SINRAS} and recovery rates for the two samples is presented in the next section.

3.5 SINRAS for Monitoring the Progress of ASR

Three parameters were extracted from SINRAS to track the progress of ASR in Glass and Oley samples: The nonlinearity parameter α_{SINRAS} (Eq. 7), the recovery rate ν (Eq. 6), and the linear resonance frequency f_0 . Similar to α_{MINRAS} , the reported values here correspond to the measurements taken at 23 °C (i.e., cold). Parameters α_{SINRAS} , ν , and f_0 at each damage level are calculated as their average values of all strong impacts ($\epsilon > 5 \times 10^{-6}$) from those 30 impacts. Similar to α_{MINRAS} , the evolution of α_{SINRAS} occurs in four phases, where α_{SINRAS} slightly decreases (Phase I), increases (Phase II), reaches a plateau (Phase III) and decreases (Phase IV)

as shown in Fig. 9a. The evolution of the second extracted parameter, the recovery rate ν for Oley and Glass specimens is depicted in Fig. 9b. Like α_{SINRAS} , the recovery rate ν clearly discriminates the two samples: it quadruples after 26 days for Glass sample, while fluctuating within a narrow range (30–70 s^{-1}) for sample Oley. The recovery rate ν is not correlated to α_{SINRAS} and does not exhibit the four phases of evolution for sample Oley. Finally, the trend of f_0 extracted from SINRAS is very similar to that from MINRAS (Fig. 7), and the error bars for f_0 are much smaller than those for nonlinear parameters (Fig. 9c). By giving three independent parameters, SINRAS provides a comprehensive assessment of the state of damage in concrete samples with minimal additional effort than that required for obtaining only f_0 using standardized approaches.

A comparison between the nonlinearity parameter α obtained from MINRAS and SINRAS shown in Fig. 10 indicates that the two sets of parameters are strongly correlated. The R squared value for uncorrected α_{MINRAS} and α_{SINRAS} is 0.934 and the R squared value corrected α_{MINRAS} and α_{SINRAS} is 0.916.

Fig. 10 There is a strong correlation between the nonlinearity parameter extracted from MINRAS and SINRAS: **a** correlation between uncorrected α_{MINRAS} and α_{SINRAS} , and **b** between corrected α_{MINRAS} and α_{SINRAS}

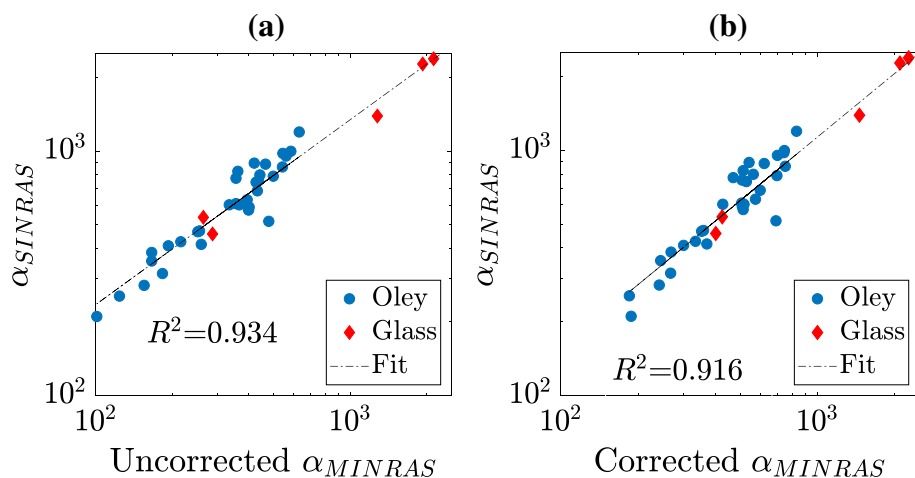
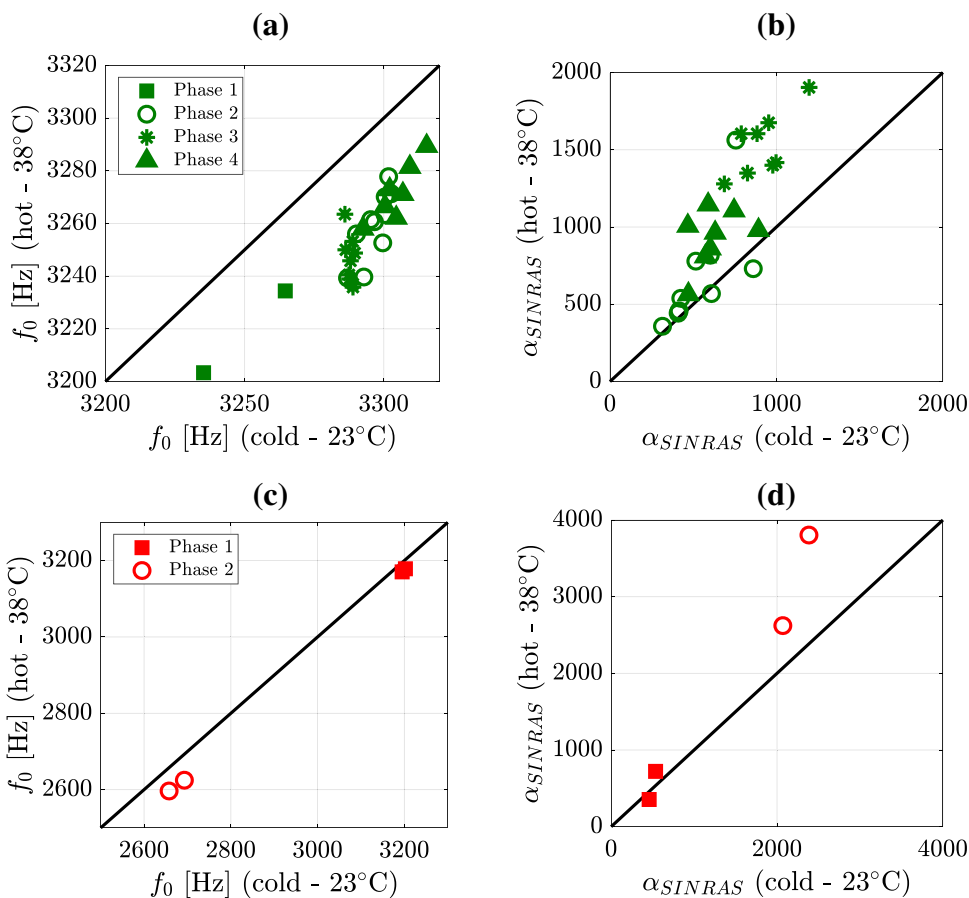


Fig. 11 A comparison between measurements at 38 °C (hot) and 23 °C (cold): linear resonant frequency f_0 for: **a** Oley, **c** Glass; and nonlinear parameter α_{SINRAS} for **b** Oley, **d** Glass during the four consecutive phases identified in Figs. 6 and 7



3.6 Influence of Temperature on f_0 and α_{SINRAS}

The measured values of f_0 , α_{SINRAS} and ν at 38 °C (hot) and 23 °C (cold) are compared in Fig. 11. Different markers are used in each panel to denote the four phases of temporal changes in f_0 and α_{SINRAS} as previously shown in Figs. 7 and 9, respectively. It is observed that f_0 at 23 °C is generally higher (0.89% on average) than that at 38 °C (Fig. 11a–c). On the other hand, the influence of temperature on the mea-

sured nonlinearity parameters α_{SINRAS} seems to depend on the progress of ASR. For Oley specimen (Fig. 11b), α_{SINRAS} at later ages (Phase III and IV) measures higher (15% on average) at the elevated temperature, while the temperature effect is less significant at early ages (Phase II). Similar observations are made for Glass sample. Our observations are in qualitative agreement with the results of the only published relevant study, where the nonlinearity of concrete (measured using a different parameter and fundamentally

different approach) with reactive aggregates was shown to increase by about 50% with increasing temperatures from 30 to 40 °C [28]. One possible explanation for the observed phenomenon is that the volumetric expansion of the specimen at a higher temperature opens the closed volumetric cracks resulting in a larger nonlinearity. Another hypothesis is that the lower viscosity of ASR gel at elevated temperatures results in an increased crack compliance and consequently, higher nonlinearity. Further investigation is needed to identify the underpinning for the observed effects.

4 Discussion

SINRAS is a rapid alternative to MINRAS for monitoring the progress of ASR in concrete. The main advantage of SINRAS over MINRAS is the fewer number of impacts necessary to carry out the test. Repeated application of sets of multiple impacts may inadvertently induce damage in test samples over the course of a monitoring experiment. Furthermore, the results of MINRAS are influenced by the time interval between the hammer blows because of conditioning and slow dynamics [41]. A strong hammer blow results in an instantaneous softening of materials (decrease in dynamic elastic modulus), causing a sharp decrease in resonance frequency (conditioning). If the induced strain is within the elastic limit, the softening is reversible: once the impact force is removed, the frequency slowly relaxes back towards the undisturbed value (slow dynamics). However, the more nonlinear is the material (for example, at later stages of damage), the longer it takes to fully recover although the recovery rate may be higher. As such, a sufficient time interval should be allocated between every two consecutive hammer blows to allow full relaxation of the specimen, or at the very least, the time interval must be kept constant to properly compare different states of damage and minimize the adverse effects of conditioning and slow dynamics on test results.

Our results indicate that MINRAS and NRAS results are in quantitative agreement and that SINRAS and MINRAS yield highly correlated nonlinearity parameter α . The normalized drop in resonance frequency is proportional to α_{MINRAS} , while the recovery rate ν potentially provides complementary information on the damage state of the test material. However, we observe large variations for measured ν , which somewhat obscure the temporal trend. The large variations might come from two sources. First, it might come from inconsistent values of f_0 calculated from the curve fitting (Eq. 6) for each impact, since the value of ν is very sensitive to the estimation of f_0 . This may be due to slow dynamics effects; the previous impacts influence the estimation of f_0 and the frequency recovery signatures of the subsequent impacts. In practice, SINRAS only requires one impact therefore, this source of error can be easily eliminated. Second,

the error might also come from the variation of impact levels. In this study, the impact is manually applied, and the average response to several relatively high intensity impacts (>5 micro-strain) is used to calculate the recovery rate ν and α_{SINRAS} . These variations can be easily minimized by using an automated testing system, where both the input force amplitude and duration could be held constant throughout the monitoring period. In that case, there would be no need for averaging; analyzing the response to a single controlled impact of sufficient strength would be sufficient.

5 Summary and Conclusions

This study presents the results pertaining to a series of impact-based NRAS tests to monitor the progress of ASR in concrete over the course of a standard accelerated test. First, we demonstrate that the results from conventional and multi-impact based NRAS are in quantitative agreement. Next, we compare multi-impact with single-impact approaches, where in the latter case, changes in frequency are monitored during the ring-down. We find that:

- The results from the two approaches strongly correlate, although not equivalent due to conditioning/slow dynamics effects.
- The single-impact method allows one to extract an additional nonlinear parameter (recovery rate ν) that may provide complementary information on the state of damage in the test material.

The SINRAS or ring-down approach may be better suited for practical applications since it requires only one impact. When applied to concrete, our results indicate that the nonlinearity parameters are very sensitive to ASR-induced microstructural modifications. While highly reactive samples exhibit manifold increase in nonlinearity, low reactive samples show a distinctly different but complex trend that is likely to result from the interplay of three competing mechanisms: (1) cement hydration; (2) the initiation of new microscopic cracks and (3) growth, coalescence or widening of cracks. Finally, sample temperature is shown to influence the test results and has to be taken into consideration when interpreting results obtained under different environmental conditions. It is important to note that the proposed nonlinear methods are not to replace linear frequency measurement, but to be used as complementary analysis. SINRAS outputs three parameters including f_0 ; a combination of these parameters can provide a comprehensive assessment of the state of damage in concrete samples with minimal additional efforts than that required to obtain f_0 only.

Acknowledgements Weilun Xi was supported through a Research Experience for Undergraduate (REU) award of Penn State's College of Engineering in Summer 2015. This support is greatly acknowledged.

References

1. NRC Information Notice 2011–2020: Concrete Degradation by Alkali–Silica Reaction (2011)
2. Stanton, T.: Expansion of concrete through reaction between cement and aggregate. *Proc. Am. Soc. Civ. Eng.* **66**, 1781–1811 (1940)
3. ASTM C1293-08b: Standard Test Method for Potential Alkali Reactivity of Aggregates (Mortar-Bar Method) (2014)
4. ASTM C1293-08b: Standard Test Method for Determination of Length Change of Concrete Due to Alkali–Silica Reaction (2015)
5. Fournier, B., Bérubé, M.-A., Folliard, K.J., Thomas, M.: Report on the Diagnosis, Prognosis, and Mitigation of Alkali–Silica Reaction (ASR) in Transportation Structures. FHWA-HIF-09-004 2 (2010)
6. Hashemi, A., Hatfield, S., Donnell, K.M., Zoughi, R., Kurtis, K.E.: Microwave NDE method for health-monitoring of concrete structures containing alkali–silica reaction (ASR) gel. In: AIP Conference Proceedings 1581, Baltimore, Maryland, USA, p. 787 (2014)
7. Donnell, K.M., Hatfield, S., Zoughi, R., Kurtis, K.E.: Wideband microwave characterization of alkali–silica reaction (ASR) gel in cement-based materials. *Mater. Lett.* **90**, 159–161 (2013)
8. Rivard, P., Saint-Pierre, F.: Assessing alkali–silica reaction damage to concrete with non-destructive methods: from the lab to the field. *Constr. Build. Mater.* **23**, 902–909 (2009)
9. Swamy, R.N., Al-Asali, M.M.: Engineering properties of concrete affected by alkali–silica reaction. *Mater. J.* **85**, 367–374 (1989)
10. Saint-Pierre, F., Rivard, P., Ballivy, G.: Measurement of alkali–silica reaction progression by ultrasonic waves attenuation. *Cem. Concr. Res.* **37**, 948–956 (2007)
11. Sargolzhai, M., Rivard, P., Rhazi, J.: Evaluation of residual reactivity of concrete cores from ASR-affected structures by non-destructive tests. *Non-destruct. Test. Civ. Eng.* **3**, 1–6 (2009)
12. Sargolzhai, M., Kodjo, S.A., Rivard, P., Rhazi, J.: Effectiveness of nondestructive testing for the evaluation of alkali–silica reaction in concrete. *Constr. Build. Mater.* **24**, 1398–1403 (2010)
13. Deroo, F., Kim, J., Qu, J., Sabra, K., Jacobs, L.J.: Detection of damage in concrete using diffuse ultrasound (L). *J. Acoust. Soc. Am.* **127**, 3315–3318 (2010)
14. Rivard, P., Ballivy, G., Gravel, C., Saint-Pierre, F.: Monitoring of an hydraulic structure affected by ASR: a case study. *Cem. Concr. Res.* **40**, 676–680 (2010)
15. Gong, P., Patton, M.E., Liu, C., Oppenheim, I.J., Greve, D.W., Harley, J.B., Junker, W.R.: Ultrasonic detection of the alkali–silica reaction damage in concrete. In: IEEE International Ultrasonic Symposium Proceeding, pp. 361–364 (2014)
16. Boukari, Y., Bulteel, D., Rivard, P., Abriak, N.-E.: Combining nonlinear acoustics and physico-chemical analysis of aggregates to improve alkali–silica reaction monitoring. *Cem. Concr. Res.* **67**, 44–51 (2015)
17. Abdelrahman, M., ElBatanouny, M.K., Ziehl, P., Fasl, J., Larosche, C.J., Fraczek, J.: Classification of alkali–silica reaction damage using acoustic emission: a proof-of-concept study. *Constr. Build. Mater.* **95**, 406 (2015)
18. Jin, J., Moreno, M.G., Riviere, J., Shokouhi, P.: Impact-based nonlinear acoustic testing for characterizing distributed damage in concrete. *J. Nondestruct. Eval.* **36**, 51 (2017)
19. Eiras, J.N., Monzó, J., Payá, J., Kundu, T., Popovics, J.S.: Non-classical nonlinear feature extraction from standard resonance vibration data for damage detection. *J. Acoust. Soc. Am.* **135**, EL82–EL87 (2014)
20. Payan, C., Ulrich, T.J., Le Bas, P.Y., Saleh, T., Guimaraes, M.: Quantitative linear and nonlinear resonance inspection techniques and analysis for material characterization: application to concrete thermal damage. *J. Acoust. Soc. Am.* **136**, 537 (2014)
21. Payan, C., Garnier, V., Moysan, J., Johnson, P.A.: Applying nonlinear resonant ultrasound spectroscopy to improving thermal damage assessment in concrete. *J. Acoust. Soc. Am.* **121**, EL125–EL130 (2007)
22. Van Den Abeele, K.E., Sutin, A., Carmeliet, J., Johnson, P.A.: Micro-damage diagnostics using nonlinear elastic wave spectroscopy (NEWS). *NDT E Int.* **34**, 239–248 (2001)
23. Van Den Abeele, K., Le Bas, P.Y., Van Damme, B., Katkowski, T.: Quantification of material nonlinearity in relation to microdamage density using nonlinear reverberation spectroscopy: experimental and theoretical study. *J. Acoust. Soc. Am.* **126**, 963–972 (2009)
24. Van Den Abeele, K., De Visscher, J.: Damage assessment in reinforced concrete using spectral and temporal nonlinear vibration techniques. *Cem. Concr. Res.* **30**, 1453–1464 (2000)
25. Johnson, P.A., TenCate, J.A., Guyer, R.A., Van Den Abeele, K.E.A.: Resonant nonlinear ultrasound spectroscopy. U.S. Patent No. 6,330,827 (2001)
26. Leśnicki, K.J., Kim, J.-Y., Kurtis, K.E., Jacobs, L.J.: Characterization of ASR damage in concrete using nonlinear impact resonance acoustic spectroscopy technique. *NDT E Int.* **44**, 721–727 (2011)
27. Lesnicki, K.J., Kim, J.-Y., Kurtis, K.E., Jacobs, L.J.: Accelerated Determination of ASR Susceptibility During Concrete Prism Testing Through Nonlinear Resonance Ultrasonic Spectroscopy. Fhwa-Hrt-13-085 (2013)
28. Moradi-Marani, F., Kodjo, S.A., Rivard, P., Lamarche, C.-P.: Effect of the temperature on the nonlinear acoustic behavior of reinforced concrete using dynamic acoustoelastic method of time shift. *J. Non-destruct. Eval.* **33**, 288–298 (2014)
29. Kodjo, A.S., Rivard, P., Cohen-Tenoudji, F., Gallias, J.-L.: Impact of the alkali–silica reaction products on slow dynamics behavior of concrete. *Cem. Concr. Res.* **41**, 422–428 (2011)
30. Chen, J., Jayapalan, A.R., Kim, J., Kurtis, K.E., Jacobs, L.J.: Rapid evaluation of alkali–silica reactivity of aggregates using a nonlinear resonance spectroscopy technique. *Cem. Concr. Res.* **40**, 914–923 (2010)
31. TenCate, J.A., Smith, E., Guyer, R.A.: Universal slow dynamics in granular solids. *Phys. Rev. Lett.* **85**, 1020–1023 (2000)
32. Kachanov, M.: Effective elastic properties of cracked solids: critical review of some basic concepts. *Appl. Mech. Rev.* **45**, 304–335 (1992)
33. Zheng, Y., Maev, R.G., Solodov, I.Y.: Nonlinear acoustic applications for material characterization: a review. *Can. J. Phys.* **77**, 927–967 (2000)
34. Ghahremani, S., Guan, Y., Radlińska, A., Shokouhi, P.: Carbonation-induced microstructural evolution of alkali-activated slag (AAS) revealed by nonlinear resonant acoustic spectroscopy (NRAS). *Adv. Civ. Eng. Mater. ASTM*. In press (2018)
35. ASTM C215-14: Standard test method for fundamental transverse, longitudinal, and torsional resonant frequencies of concrete specimens. (2014)
36. Guyer, R.A., Johnson, P.A.: Nonlinear mesoscopic elasticity: evidence for a new class of materials. *Phys. Today* **52**, 30–36 (1999)
37. Guyer, R., Johnson, P.: *Nonlinear Mesoscopic Elasticity: The Complex Behaviour of Rocks, Soil, Concrete*. Wiley, Berlin (2009)
38. Dahlen, U., Ryden, N., Jakobsson, A.: Damage identification in concrete using impact non-linear reverberation spectroscopy. *NDT E Int.* **75**, 15–25 (2015)
39. Carrión, A., Genovés, V., Pérez, G., Payá, J., Gosálbez, J.: Flipped accumulative non-linear single impact resonance acoustic spec-

- troscopy (FANSIRAS): a novel feature extraction algorithm for global damage assessment. *J. Sound Vib.* **432**, 454–469 (2018)
40. Renaud, G., Talmant, M., Callé, S., Defontaine, M., Laugier, P.: Nonlinear elastodynamics in micro-inhomogeneous solids observed by head-wave based dynamic acoustoelastic testing. *J. Acoust. Soc. Am.* **130**, 3583–3589 (2011)
 41. TenCate, J.A.: Slow dynamics of earth materials: an experimental overview. *Pure Appl. Geophys.* **168**, 2211–2219 (2011)
 42. Vakhnenko, O.O., Vakhnenko, V.O., Shankland, T.J., TenCate, J.A.: Soft-ratchet modeling of slow dynamics in the nonlinear resonant response of sedimentary rocks. *AIP Conf. Proc.* **838**, 120–123 (2006)
 43. Johnson, P., Sutin, A.: Slow dynamics and anomalous nonlinear fast dynamics in diverse solids. *J. Acoust. Soc. Am.* **117**, 124–130 (2005)
 44. Salwocki, S.B.: Novel Performance Tests for Evaluation of Alkali–Silica Reaction. Master’s thesis (2016)
 45. Rashidi, M., Knapp, M.C.L., Hashemi, A., Kim, J., Donnell, K.M., Zoughi, R., Jacobs, L.J., Kurtis, K.E.: Detecting alkali–silica reaction: a multi-physics approach. *Cem. Concr. Compos.* **73**, 123–135 (2016)
 46. Leśnicki, K.J., Kim, J.-Y., Kurtis, K.E., Jacobs, L.J.: Assessment of alkali–silica reaction damage through quantification of concrete nonlinearity. *Mater. Struct.* **46**, 497–509 (2013)
 47. Thomas, M., Fournier, B., Folliard, K., Ideker, J., Shehata, M.: Test methods for evaluating preventive measures for controlling expansion due to alkali–silica reaction in concrete. *Cem. Concr. Res.* **36**, 1842–1856 (2006)
 48. Van Damme, B., Van Den Abeele, K.: The application of nonlinear reverberation spectroscopy for the detection of localized fatigue damage. *J. Nondestruct. Eval.* **33**, 263–268 (2014)

Publisher’s Note Springer Nature remains neutral with regard to jurisdictional claims in published maps and institutional affiliations.